Determination of solid surface tension from particle–substrate pull-off forces measured with the atomic force microscope

Jaroslaw Drelich [a,*], Garth W. Tormoen [a], Elvin R. Beach [b]

[a] *Department of Materials Science and Engineering, Michigan Technological University, Houghton, MI 49931, USA*
[b] *The Dow Chemical Company, Analytical Sciences, 1897 Bldg., Midland, MI 48640, USA*

Abstract

Atomic force microscopy (AFM) is capable of solid surface characterization at the microscopic and submicroscopic scales. It can also be used for the determination of surface tension of solids (γ) from pull-off force (F) measurements, followed by analysis of the measured F values using contact mechanics theoretical models. Although a majority of the literature γ results was obtained using either Johnson–Kendall–Roberts (JKR) or Derjaguin–Muller–Toporov (DMT) models, re-analysis of the published experimental data presented in this paper indicates that these models are regularly misused. Additional complication in determination of γ values using the AFM technique is that the measured pull-off forces have poor reproducibility. Reproducible and meaningful F values can be obtained with strict control over AFM experimental conditions during the pull-off force measurements (low humidity level, controlled and known loads) for high quality substrates and probes (surfaces should be free of heterogeneity, roughness, and contamination). Any probe or substrate imperfections complicate the interpretation of experimental results and often reduce the quality of the generated data. In this review, surface imperfection in terms of roughness and heterogeneity that influence the pull-off force are analyzed based upon the contact mechanics models. Simple correlations are proposed that could guide in selection and preparation of AFM probes and substrates for γ determination and selection of loading conditions during the pull-off force measurements. Finally, the possibility of AFM measurements of solid surface tension using materials with rough surfaces is discussed.

© 2004 Elsevier Inc. All rights reserved.

Keywords: Atomic force microscopy; Chemical force microscopy; Adhesion; Surface energy; Surface tension

1. Introduction

Many modern materials possess surfaces that are engineered to have special wetting, electronic, optical, and other properties. Material modification is often accomplished through an alteration of the material surface region at a depth of a single atomic or molecular layer to several micrometers. This can be achieved by adsorption of organic modifiers, deposition of thin inorganic or organic films, surface etching, initiation of chemical reaction at the surface, etc. Many engineered surfaces cannot be melted, dissolved, or fractured, therefore their surface/interfacial tension (γ) cannot be de-

termined through any of the "conventional" techniques such as tensiometry, solubility studies, crystal cleavage, zero-creep method, etc. The theoretical background and experimental techniques for solid's surface tension determination have been reviewed previously [1,2] and will not be repeated here. Additionally, these conventional techniques are usually applicable to macroscopic solids, whereas the current trend in miniaturization of products and devices pose the need for examination of nanosurfaces or surfaces with nanoscale characteristics. New γ determination methods need to be developed to meet these needs. Two techniques based on either (i) contact angles for macroscopic surfaces [3] or (ii) adhesion force measurements for microscopic and submicroscopic surfaces by AFM [4] have been under intensive development by several research groups in recent years.

---

* Corresponding author.
  E-mail address: jwdrelic@mtu.edu (J. Drelich).

The experimental approach to determine γ of solids based on contact angle measurements is relatively simple for flat, smooth, homogeneous, and inert macroscopic substrates. Problems arise with substrates that are: (i) reactive with, or sensitive to, the environment (common case for solids in contact with many liquids or solutions), and/or (ii) have small dimensions (e.g., small or powdered samples, patterned heterogeneous substrates with microscopic domains). In other words, the contact angle measurement technique is limited to materials that are stable in the environment of the probing liquids. Any ionization of functional groups, chemical instability of the solid, or dissolution of the solid by the probing liquid invalidates this method for γ determination. Also, the interfacial tension between a solid and a solution cannot be deduced from contact angle measurement results. Additionally, the contact angle technique probes "average" surface properties of heterogeneous surfaces and thus, is unable to distinguish the discrete nature of such surfaces at the microscopic and submicroscopic levels. The direct method of pull-off force measurements using the atomic force microscope is a very attractive technique for surface characterization of such engineered materials.

In this paper, we first briefly discuss the basics of the AFM technique for the determination of the solid surface tension and then, discuss common technical problems faced by the researchers during normalization and interpretation of the AFM pull-off force measurements. The AFM pull-off force measurements have not been widely accepted for measurements of γ of solids because of an irreproducible nature of the data generated by this approach. Factors such as varying surface roughness and heterogeneity characteristics of both probes and substrates, and varying loads/deformation of the tip and substrate are among the major reasons for widely scattered data, even for the same set of materials used in a single experiment. Strict control of all of these conditions should be recognized. This paper reviews progress on application of the AFM technique as an analytical tool in measurements of surface tension of engineered surfaces, and several new aspects of these measurements are presented in this paper.

2. Measurements of pull-off forces using atomic force microscopy

2.1. Basics of the AFM technique

The principles of the AFM are well described in the literature [4–6]; here, the major features of surface force measurements are reviewed. The AFM measures the deflection of a cantilever spring with a sharp cantilever tip (tip radius is usually 10 to 100 nm) or an attached particle (a particle with a diameter ranging from about 2 to more than 20 μm is glued to the end of the cantilever) as a function of displacement from a horizontal position. The deflection, monitored by a laser–photodiode system, relates to the forces acting be-
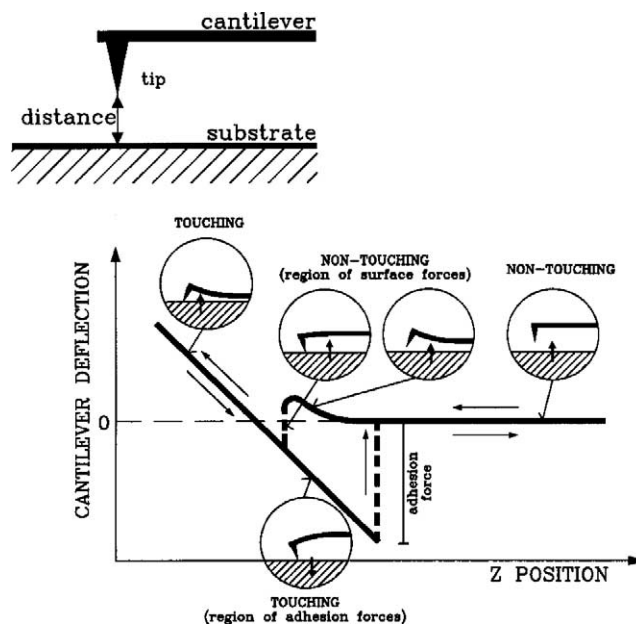

Fig. 1. Schematic of a cantilever deflection vs vertical position of cantilever curve in the AFM measurement of surface forces.

tween a probing tip and a substrate. Fig. 1 shows a schematic of the cantilever deflection vs tip–substrate distance curves and Fig. 2 shows two examples of cantilever tips.

As shown in Fig. 1, the AFM measurement starts at a large tip–surface separation in the so-called nontouching regime. Then with or without a slight deflection, depending on the long-distance tip–surface interactions, the surface approaches the tip following the horizontal line moving right to left in the force vs distance curve. At a certain point, when the tip–substrate attractive interactions overcome the stiffness of the cantilever, the transition from nontouching to touching occurs, and the tip "jumps" onto the sample surface.

Moving the substrate (surface) still further causes deflection of the cantilever equal to the distance that the substrate is moved. This is referred to as the touching regime or constant compliance region represented by the diagonal line in the left part of the force vs distance curve. Upon retracting the surface from the tip, i.e., going toward the right in the force vs distance curve, the cantilever again moves with the surface. The cantilever deflects toward the surface due to adhesion force before the tip breaks contact with the surface, going through the lowest point in the force vs distance curve. At this "jump-off" point, the tip completely loses contact with the surface, and the cycle is complete. The force required to pull the tip off the substrate surface is called *pull-off* or *adhesion force* (F) and is calculated from Hooke's law,

$$F = k\Delta x, \tag{1}$$

where k is the spring constant of cantilever and Δx is the maximum deflection of cantilever during tip–substrate adhesion.
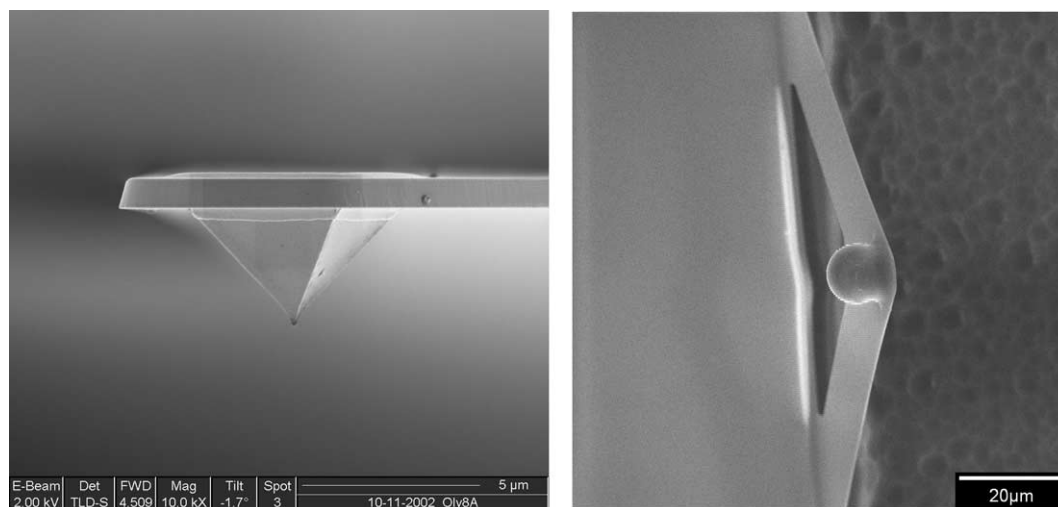
Fig. 2. Scanning electron micrographs of a cantilever tip (left) and colloidal probe (borosilicate glass) glued to a tipless cantilever (right).

Accuracy of the F measurement, which directly relates to the solid surface tension (as will be shown later), depends on the precision of which both the spring constant of cantilever and its deflection during pull-off force measurements are determined. The laser beam–photodiode detector systems of the AFM instruments are usually capable of recording deflection of the cantilever to subangstrom precision and the major error in pull-off force determination is associated with the k value determination. This error, however, is constant and cannot cause a scatter of F values, always reported in the literature even for the highest quality and most carefully prepared probes and substrates. Standard deviation from 10% to 20% of an average value is commonly reported. Errors in piezo responses resulting from piezo hysteresis and creep, as well as fluctuation of light intensity and its interference, may cause variations in the F value determination. Nevertheless, the major causes for the scatter of F values are imperfections in solid surfaces of both substrates and probes and uncontrolled deformations of the materials posed by uncontrolled and varied loading conditions. We will return to these issues in a later part of this paper.

2.2. Cantilever's spring constant

Two basic types of cantilevers, triangular (V-frame) and single beam cantilevers (rectangular or trapezoidal) [5,6], commonly used for imaging of substrate topography, are also used for force measurements. V-frame cantilevers are made of polycrystalline silicon or silicon nitride. They come available with a variety of elastic constants, from a fraction of N/m to several N/m. Single beam silicon cantilevers are stiffer with spring constants varying from several N/m to tens of N/m. The expected strength of the adhesion between the tip of the cantilever and a substrate dictates the choice of cantilever (i.e., strong adhesion forces require cantilevers with large spring constants).

Estimates for the cantilever spring (elastic) constant for every type of cantilever is provided by the manufacturer. The

values specified by producers are however, average spring constants, usually determined for a batch of cantilevers. Small variations in the dimensions of the cantilever during manufacture result in significant changes in k, therefore, the spring constant for each cantilever may deviate from the specified average value by as much as 10–20% for V-frame cantilevers (which are very regular in shape) and up to 100% for single beam cantilevers (which are more irregular in shape). In quantitative force studies, such as those discussed in this paper, it is necessary to determine the cantilever spring constant more accurately.

Among several proposed approaches, three methods are commonly used for the spring constant determination (see Ref. [7] for review). The first method is based on conventional static mechanics, and the spring constant is calculated from the cantilever dimensions and Young's modulus of the materials used for cantilever fabrication [7]. This method is more suitable for cantilevers that are regular in shape and requires that the material properties are known and uniform over the entire cantilever. The presence of submicroscopic defects are detrimental to mechanical properties of microscopic cantilevers and can cause deviation from what is expected for bulk material. The thickness of a coating (gold, for example), if applied, must also be known.

A second method relies on measurement of the resonant frequency of the cantilever before and after an end-mass is attached [8]. A spherical particle, typically tungsten, is attached to the cantilever through capillary forces. A drawback of this nondestructive method is that particles often do not stay attached to the cantilever without glue. Also, precise weights of particles are required for accurate determination of k.

A third method is called the thermal noise method [9]. Although this method is restricted to cantilevers with $k < 1$ N/m, it has became very popular among service laboratories. This method relies on measurements of mean square displacement of the unloaded cantilever due to thermal mo-

tion. The details of this method as well as two other above-mentioned methods are reviewed by Sader [7].

These days, precalibrated cantilevers can be purchased from several companies and this task is usually no longer necessary for researchers. It should be recognized, however, that the experimental spring constants are always determined with limited precision and errors of typically 5–10% are encountered, though a 20% error is not unusual.

3. Correlation between pull-off force and solid surface tension

The equilibrium work of adhesion (W_A) is defined by the negative of the Gibbs free energy change per unit area (ΔG) of interacting interfaces, and is expressed by the Dupré equation [3],

$$W_A = -\Delta G = \gamma_{13} + \gamma_{23} - \gamma_{12}, \tag{2}$$

where subscripts 1, 2, and 3 describe three different phases of the system: solid 1, solid 2, and fluid.

If we replace one surface with a spherical particle (or probing tip), such as the systems used in AFM studies, the relation between the work of adhesion and adhesion (pull-off) force (F) can be described by the Derjaguin approximation,

$$F = 2\pi R W_A, \tag{3}$$

which is applicable to perfectly rigid particles in contact. The Derjaguin approximation is valid for systems where the separation distance between the sphere and substrate is much shorter than the radius of the sphere (probe). In measurements of adhesion forces this assumption always applies, but this approximation can fail in the examination of (long-range) noncontact forces. It is important to note that in reality, particles and/or substrates deform elastically and/or plastically under applied loads during adhesion, and particle–substrate analysis requires more accurate contact mechanics models that include a physical deformation component.

In AFM pull-off force measurements, continuum contact mechanics models are commonly used to describe the probe–substrate system with a high degree of ideality. Typical AFM measurements utilize either spherical particles glued to cantilevers or commercial cantilever tips with rounded ends and such systems are modeled as a sphere in contact with a flat surface. Many practical systems deviate from this idealized geometry, often causing problems in interpretation of measured AFM pull-off forces. As a result, significant effort is always concentrated on preparation of as close-to-perfect sphere–flat systems as possible in order to simplify the analysis of experimental pull-off force results. However, this has not always been accomplished and many literature reports lack complete characterization of probes and substrates (i.e., probe geometry and dimension, probe and substrate surface roughness, probe and substrate surface heterogeneity, etc.).

Two contact mechanics models derived by Johnson et al. [10] and Derjaguin et al. [11], named JKR and DMT models, respectively, are frequently used by researchers to interpret the pull-off forces measured by the AFM technique. These analytical models were reviewed in detail by many authors [4,12–16] and will not be repeated here. In general, both JKR and DMT models apply to particle–substrate systems where the following assumptions are met: (i) deformations of materials are purely elastic, described by classical continuum elasticity theory, (ii) materials are elastically isotropic, (iii) both Young's modulus and Poisson's ratio of materials remain constant during deformation, (iv) the contact diameter between particle and substrate is small compared to the diameter of particle, (v) a paraboloid describes the curvature of the particle in the particle–substrate contact area, (vi) no chemical bonds are formed during adhesion, and (vii) contact area significantly exceeds molecular/atomic dimensions.

The difference between JKR and DMT models occurs in assuming the nature of forces acting between particle and substrate. Johnson et al. [10] assumed in their model that attractive forces act only inside the particle–substrate contact area, whereas Derjaguin et al. [11] included long-range surface forces operating outside the particle–substrate contact area. Both JKR and DMT models describe the correlation between pull-off force (F) and work of adhesion (W_A) through a simple analytical equation of the following form,

$$F = c\pi R W_A, \tag{4}$$

which leads to Eq. (5) for a symmetrical system (when interacting materials and their surfaces are the same):

$$\gamma = \frac{F}{2c\pi R}. \tag{5}$$

R is the radius of the particle (probing tip) and c is a constant; $c = 2$ in the DMT model and $c = 1.5$ in the JKR model. Thus, knowing which contacts mechanics model applies to a particular system under study, and setting operation conditions during the AFM measurements that satisfy the particular model, the γ value can be determined. Note that (i) both models, JKR and DMT, were derived based on the Hertz theory [17], and (ii) an analytical solution to the DMT model was provided by Maugis [16].

Which of the contact mechanics models should be selected for interpretation of the AFM pull-off forces is not always straightforward. In general, the DMT model is more appropriate for systems with hard materials having low surface energy and small radii of probe curvature. The JKR model applies better to softer materials with higher surface energy and larger probes. This generalization, however, does not bring the researcher any closer to the selection of the appropriate model and mistakes are often made (including our own).

Maugis analyzed both the JKR and DMT models and suggested that the transition between these models can be pre-

dicted from the dimensionless parameter λ defined as [16]

$$\lambda = \frac{2.06}{z_0} \sqrt[3]{\frac{R W_A^2}{\pi K^2}}, \tag{6}$$

where z_0 is the equilibrium separation distance between the probe and substrate, R is the radius of the probe, W_A is the work of adhesion, and K is the reduced elastic modulus for the particle–substrate system where

$$\frac{1}{K} = \frac{3}{4} \left(\frac{1 - \nu_p^2}{E_p} + \frac{1 - \nu_s^2}{E_s} \right); \tag{7}$$

ν is the Poisson ratio and E is the Young's modulus, and p and s stand for probe (particle) and substrate, respectively.

For $\lambda \to \infty$ ($\lambda \geqslant 5$) the JKR model applies whereas the DMT model is more appropriate for systems with $\lambda \to 0$ ($\lambda \leqslant 0.1$). The transition between these two models is described by the Maugis–Dugdale (MD) theory [16]. Often for AFM pull-off force measurements, the MD model seems to be more appropriate than either of the JKR or DMT models as will be shown in the next section.

In the MD model, two parametric equations must be solved to describe the transition region between JKR and DMT mechanics. These equations are [16]

$$\bar{P} = \bar{A}^3 - \lambda \bar{A}^2 \left(\sqrt{m^2 - 1} + m^2 \cos^{-1}\left(\frac{1}{m} \right) \right), \tag{8}$$

$$\frac{\lambda \bar{A}^2}{2} \left[\sqrt{m^2 - 1} + (m^2 - 2) \cos^{-1}\left(\frac{1}{m} \right) \right]$$
$$+ \frac{4 \lambda^2 \bar{A}}{3} \left[-m + 1 + \sqrt{m^2 - 1} \cos^{-1}\left(\frac{1}{m} \right) \right] = 1, \tag{9}$$

where $m = b/a$ is the ratio between an outer radius at which the adhesive stress no longer acts in the gap between the surfaces and the contact radius; $\bar{P}$ and $\bar{A}$ are the normalized load and normalized radius of the contact area, respectively:

$$\bar{P} = \frac{P}{\pi R W_A}, \tag{10}$$

$$\bar{A} = \frac{a}{(\pi R^2 W_A / K^2)^{1/3}}. \tag{11}$$

A problem with this model is that there is no single expression between a and P and both Eqs. (8) and (9) must be solved simultaneously. Importantly, there is also no simple relation for pull-off force and iteration is needed to calculate the c value ($1.5 < c < 2$) in Eq. (4). Examples of calculated c values for different λ parameters are presented in [18].

4. Solid surface tension values determined by the AFM technique: critical literature review

Table 1 summarizes a number of data reported in the literature for adhesion force measurements made with atomic force microscopy. This table includes data from pull-off force measurements for AFM cantilever tips, both unmodified and coated tips, as well as for some colloidal probes,

performed either in liquid or gaseous environments. As for substrates, gold films modified with organic functionality, polymers, and inorganic materials were used in the AFM experiments. The spring constant is shown in Table 1 to derive possible loading conditions experienced during measurement, a parameter often left unreported. In addition, the contact mechanics model used by the authors to calculate the work of adhesion (W_A) along with the reported W_A is included. This is contrasted with what is predicted for W_A from contact angle determinations of surface tension components for the tested materials. The final four columns depict calculations performed for the tested systems in order to determine what constant (c) is appropriate for determining W_A from force measurements, according to the MD model [16]. In this contribution, we used the approach proposed by Carpick et al. [18] in determination of the c parameter. The corresponding recalculated W_A value is shown in the last column of the table.

Table 2 shows the material properties used in calculations of the reduced elastic modulus (K) for the probe–substrate systems presented in Table 1. Finally, Table 3 shows the calculated K values. Note that for self-assembled monolayers, the material properties of the underlying substrate were used to determine K and not the properties of the monolayer films themselves due to the small thicknesses (1–1.5 nm) and expected pliancy of the monolayers.

As shown in Table 1, both continuum contact mechanics models, the JKR model and DMT model, were used in analysis of the measured pull-off forces, although selection of a particular model was rarely justified. Also, based on the literature reports there is no clear distinction between analysis of the data generated with sharp tips and colloidal probes, in spite of the fact that both the size of the probe and spring constant of cantilever differ significantly in both cases. Additionally, although we do not analyze all details of previous experimental work, we noted that many papers also lack reporting of mechanical properties of materials used in experimentation and loads that are used during pressing the tip or colloidal probe on the substrate surface. This information is important for detailed analysis of the pull-off forces and behavior of the tip–substrate system.

The calculated values of the Maugis parameter (λ) for the literature systems (Table 1) indicate that a common characteristic in a majority of publications is the use of an incorrect contact mechanics model for analysis of pull-off forces and subsequent calculation of the work of adhesion or surface energy. The JKR model was used most frequently in analysis of pull-off forces obtained with colloidal probes coming in contact with various substrates. Although the selection of the JKR model for analysis of the results from colloidal probe microscopy studies is often appropriate, this selection should not be blindly made without analysis of the λ parameter; examples of the systems where the MD model is more appropriate are shown in Table 1. Also, the JKR model was the most popular in analysis of pull-off forces measured with sharp tips (regular and coated), in spite of the fact that the

Table 1
Measured and calculated values of the work of adhesion for different systems

Ref.	System		Probe		Lit. results			This study			
	Surface chemistry	Medium	R [nm] or [µm]	k [N/m]	W_A [mJ/m²] Predicted	Determined	Model used	K [GPa s]	λ ($z=$ 0.2–0.4 nm)	c	W_A [mJ/m²]
Sharp tips (R in [nm])											
Noy et al. [19]	COOH–COOH	Ethanol	54	0.12	ND	8.9 ± 3.1	JKR	64.4	0.04–0.07	2.0	6.7 ± 2.3
	CH_3–CH_3				5	3.9 ± 1.5	$c = 1.5$	64.4	0.03–0.06	2.0	2.9 ± 1.1
Van der Vegte and Hadziioan-nou [20]	CH_3–CH_3	Ethanol	35	0.2	5	5	JKR	64.4	0.03–0.05	2.0	3.8
	CH_3–CH_3	Water			104	103	$c = 1.5$	64.4	0.2–0.4	1.8	86
	OH–OH	Ethanol			ND	6		64.4	0.02–0.04	2.0	2.3
	NH_2–NH_2	Ethanol			ND	5.6		64.4	0.01–0.03	2.0	2.1
	COOH–COOH	Ethanol			ND	9		64.4	0.03–0.05	2.0	3.4
	$CONH_2$–$CONH_2$	Ethanol			ND	10.6		64.4	0.03–0.06	2.0	4.0
Tsukruk and Bliznyuk [21]	SiOH–SiOH	Water	40–500	0.23–0.25	ND	4	JKR	ND	ND	ND	ND
	Si_3N_4–Si_3N_4					8	$c = 1.5$	220.7	0.01–0.06	2.0	6
	NH_2–NH_2					4.5		76.9	0.02–0.08	2.0	3.4
	SO_3H–SO_3H					1.5		76.9	0.01–0.04	2.0	1.1
	CH_3–CH_3					0.5		76.9	< 0.02	2.0	0.4
Clear and Nealy [22]	CH_3–CH_3	Hexadecane	∼60	0.44	1.6	4.1	JKR	70.2	0.02–0.03	2.0	3.1
		Ethanol			5.5	3.3	$c = 1.5$	70.2	0.03–0.07	2.0	2.5
		1,2-Propanediol			27.1	20.7		70.2	0.1–0.2	1.9	16.3
		1,3-Propanediol			43.7	41.5		70.2	0.13–0.27	1.9	32.8
		Water			102.8	102.9		70.2	0.24–0.47	1.8	85.8
	COOH-ox-OYTS	Hexadecane			ND	19.6		70.2	0.1–0.2	1.9	15.5
		Ethanol			ND	10.1		70.2	0.04–0.08	2.0	7.6
		1,2-Propanediol			ND	16		70.2	0.05–0.1	2.0	12
		1,3-Propanediol			ND	6		70.2	0.03–0.07	2.0	4.5
		Water			ND	1.7		70.2	0.01–0.02	2.0	1.3
	COOH–COOH	1,2-Propanediol			ND	14		70.2	0.05–0.09	2.0	10.5
		1,3-Propanediol			ND	14.6		70.2	0.05–0.1	2.0	11
	CH_3-ox-OYTS	Hexadecane			ND	4.6		70.2	0.02–0.04	2.0	3.5
		Ethanol			ND	2.1		70.2	0.01–0.03	2.0	1.6
		1,2-Propanediol			ND	4.9		70.2	0.02–0.04	2.0	3.7
		1,3-Propanediol			ND	6		70.2	0.03–0.07	2.0	4.5
		Water			ND	0.9		70.2	0.01–0.02	2.0	0.7
El Ghzaoui [23]	SiO_2–PTFE	Dry N_2	70	NA	95	88	DMT	0.7	1.7–3.4	1.6	110
	SiO_2–PP				110	114	$c = 2$	2	1.0–2.0	1.6	142
	SiO_2–PU				145	150		∼(1–2)	∼(1–2)	1.6	187
Skulason and Friesbie [24]	CH_3–CH_3	Water	15–130	0.23–0.28	103	110 ± 10	JKR $c = 1.5$	64.4	0.16–0.64	1.8	92 ± 8
Jaquot and Takadoum [25]	Si_3N_4–silica	Water	200	0.3	27.9	30	DMT	99.9	0.1–0.2	1.9	32
	Si_3N_4–TiN				20	18.3	$c = 2$	ND	ND	ND	ND
	Si_3N_4–DLC				13.5	12		337.7	0.03–0.06	2.0	12
	Si_3N_4–Si(111)				27.5	42		114.1	0.1–0.2	1.9	44
	Si_3N_4–Si(100)				19.9	24		114.1	0.09–0.2	1.9	25
Leite et al. [26]	Si–mica	Water	23	0.13	110	83	DMT	36.6	0.3–0.6	1.8	92
	Si–mica	Air			215	173	$c = 2$	36.6	0.4–0.9	1.7	204
Colloidal probes (R in [µm])											
Burnham et al. [27]	W–mica	Dry N_2	2.5 ± 0.5	50 ± 10	369	21	DMT	44.4	2.4–4.8	1.5	28
	W–graphite				210	14	$c = 2$	ND	ND	ND	ND
	W–Al_2O_3		2.0 ± 0.5		128	8		286	0.3–0.8	1.7	9.4
	W–CH_3				98	3		286	0.3–0.6	1.8	3.3
	W–CF_3		2.5 ± 0.5		96	1		286	0.3–0.7	1.8	1.1
	W–PTFE		2.0 ± 0.5		92	0		0.7	15–35	1.5	ND

Table 1 (*continued*)

Ref.	System		Probe		Lit. results			This study			
	Surface chemistry	Medium	R [nm] or [µm]	k [N/m]	W_A [mJ/m²] Predicted	Determined	Model used	K [GPa s]	λ ($z =$ 0.2–0.4 nm)	c	W_A [mJ/m²]
Biggs and Spinks [28]	PS–mica	Dry N_2	5	27 ± 1	102.4	148.5/122.5	JKR/MP	4	7–14	1.5	148.5
Nalaskowski et al. [29]	PE–SiO_2	Water	5–9	27–30	21	4.4	JKR	2	2–7	1.5	4.4
	PE–SiO_2 (heat)				35	21	$c = 1.5$		4–8	1.5	21
	PE–CH_3				66	64			6–12	1.5	64

Table 2
Elastic modulus and Poisson's ratio for materials analyzed in this study

Material	Young's modulus [GPa]	Poisson's ratio	Source
Au	78	0.44	[30]
W	411	0.28	[30]
PS	2.8–3.5	0.38	[31]
PP	1–1.6	0.4 (assumed)	[31]
PTFE	0.41	0.46	[31]
Mica	34.5	0.205	[32]
Si	107	0.27	[33]
Si_3N_4 (hot pressed)	300–330	0.22	[33]
SiO_2	94	0.17	[33]
Diamond	1035	0.1–0.29	[34]
Al_2O_3	390	0.2–0.25	[33]

Table 3
Reduced elastic moduli for AFM systems reported in the literature

System	$1/K$	K [GPa]
Au–Au	1.55077×10^{-11}	64.4
Si–Si	1.29967×10^{-11}	76.9
Si_3N_4–Si_3N_4	4.53143×10^{-12}	220.7
W–mica	2.25073×10^{-11}	44.4
W–PTFE	1.53827×10^{-9}	0.7
PS–mica	2.50004×10^{-10}	4.0
Si–mica	2.73239×10^{-11}	36.6
Si_3N_4–Si	8.76408×10^{-12}	114.1
Au–Si	1.42522×10^{-11}	70.2
W–Al_2O_3	3.5031×10^{-12}	285.5
Si_3N_4–SiO_2	1.00139×10^{-11}	99.9
Si_3N_4–DLC	2.96137×10^{-12}	337.7
SiO_2–PTFE	1.44994×10^{-9}	0.7
SiO_2–PP	4.92364×10^{-10}	2.0

small dimensions of the tips comply better with the assumption of the DMT model. As shown in Table 1, the results of chemical force microscopy studies (sharp tips modified with organic functionality) can usually be analyzed by the DMT model. This again cannot be assumed a priori, and systems with softer substrates such as polymers require analysis with either the MD model or JKR model.

5. Common sources of experimental errors (and misconceptions)

5.1. Characterization of the AFM probes

One of the key to a successful understanding of pull-off forces measured by AFM, and establishment of their relation with surface tensions, is a detailed characterization of the system under investigation including both shape and size of the probe tip. Conventional cantilevers have tips made of only two type of materials, silicon or silicon–nitride, therefore tips are often modified or replaced with particles (as discussed in the previous section) to broaden the spectrum of materials that can be studied with the AFM technique. The tip material may be altered by coating with a thin film of metal, however, due to high surface energies of metals, the control of their surface chemistry is difficult. For example, oxide films grow very fast on a majority of deposited metals. Organic contaminants also adsorb very quickly on both metals and oxides when exposed to a regular laboratory environment. It is also possible to form coatings of poly-

meric materials on the cantilever tips, although researchers have not explored this option, mainly due to the dangers of depositing polymer on the cantilever leg, which can cause problems with reflection of the laser beam and affect bending of the cantilever.

Silicon or silicon nitride surfaces can be directly modified with (organic) silanes, but the quality of the adsorbed molecular layers is often questionable. Instead, tips are usually coated with a thin film of gold, which is next modified with self-assembled monolayers (SAMs) of thiols with a desirable functionality. SAMs of thiols (X–$(CH_2)_n$–SH) form a very regular, close-packed structure by reacting the –SH end group with a gold surface whereas the other end group (X: CH_3, OH, COOH, NH_2, and others) is exposed to the environment. Force measurements made with SAM-modified tips are categorized as chemical force microscopy (CFM) and have become an area of intensive fundamental research [35,36].

A small particle with a diameter of 2 to 20 µm (or even larger) can also be attached to the cantilever, typically by gluing or in some cases melting the particle to the cantilever (we follow previous reports and call such probes "colloidal probes" in many parts of this paper, although the size of such probes are larger than frequently accepted size of colloids, $\leqslant 1$ µm). Both tipless cantilevers and cantilevers with regular tips are used for this purpose. This allows nearly limitless combinations of materials to be used in force testing.

Fig. 2 shows example of both a commercial tip and a colloidal probe.

A problem with manufacturing of colloidal probes is that not many materials are commercially offered in the shape of small spherical particles, and often a new methodology of colloidal particle precipitation, characteristic to that particular material (as, for example, in [37,38]), must be developed for this purpose. This is not practical for some materials, therefore force measurements have been carried out with irregular particles [39–41], which make quantification and interpretation of the experimental data difficult or even impossible. Even "spherical" particles can show rough surfaces at the nanoscale that can affect the contact area between the probe and substrate during the AFM pull-off force measurements.

Characterization of the probe size and its shape, including determination of surface defects and nanoroughness at the tip apex, is an important task for analysis of the results from AFM pull-off force measurements. The radius of curvature for AFM cantilever tips are less than 100 nm and standard thermionic emission scanning electron microscopes (SEMs) cannot resolve the edges of such small features without reducing the signal to noise ratio to the point that the object is indistinguishable from the background. Field emission SEM (FE-SEM) techniques have much better resolution than thermionic emission SEM, and are often used to characterize the AFM tip shape and topography. Two alternative methods, both utilizing the AFM instrument, are used in our laboratory.

First, larger (colloidal) probes can be imaged directly with another (much sharper) AFM cantilever using Tapping-Mode AFM imaging. Fig. 3 shows an image of a polyethylene microsphere obtained by this technique. A problem with this approach is that positioning of the scanning cantilever tip over the top of the colloidal probe is difficult using the optical microscope attached to the AFM instrument. Also it is difficult to keep the cantilever solid and stable during imaging.

Second, the technique called *blind tip reconstruction* (BTR), developed by Villarubia [42], is more versatile and used frequently in our laboratory. In BTR, either the AFM tip or colloidal probe is scanned over an ultrasharp silicon grating (specially fabricated array of sharp silicon spikes or asperities such as in TGT or TGG gratings, respectively, offered by NT-MDT Co., Moscow, Russia). The grating features must have a higher aspect ratio than the shape of the AFM tip in order to produce an inverted image of the tip rather than the image of the spike/asperity. Also, radii of the grating feature tip or edge should be small (they are less than 10 nm for TGT and TGG).

Using (Deconvo) software based on mathematical morphology operations (NT-MDT Co.), the radius of curvature of the tip is determined from images generated by the BTR method. Fig. 4 shows an example of AFM image and corresponding cross section of this image produced by scanning the colloidal probe made of borosilicate glass over the TGT grating.

Noise artifacts in the image have a large influence on the results of BTR experiments. Low scan rates should be used and the AFM instrument should be placed on an antivibration support; a cement plate suspended by bungee cords (offered by Digital Instruments) is probably the best choice in eliminating vibrations. Even after such precautions, sharp changes in height of the grating features can produce artifacts in the image [36]. An additional complication in the BTR method is the possibility for scratching of the probe with the harder silicon spike/asperity. To avoid scratching, probe–contact forces during imaging should be minimized.

5.2. Plastic deformation of the probe

As shown in Fig. 5, the probe can be severely damaged during the pull-off force measurements. Loads and frictions experienced by the probe during multiple contacts with substrate can induce plastic deformation in the material, or simply fracture the tip.
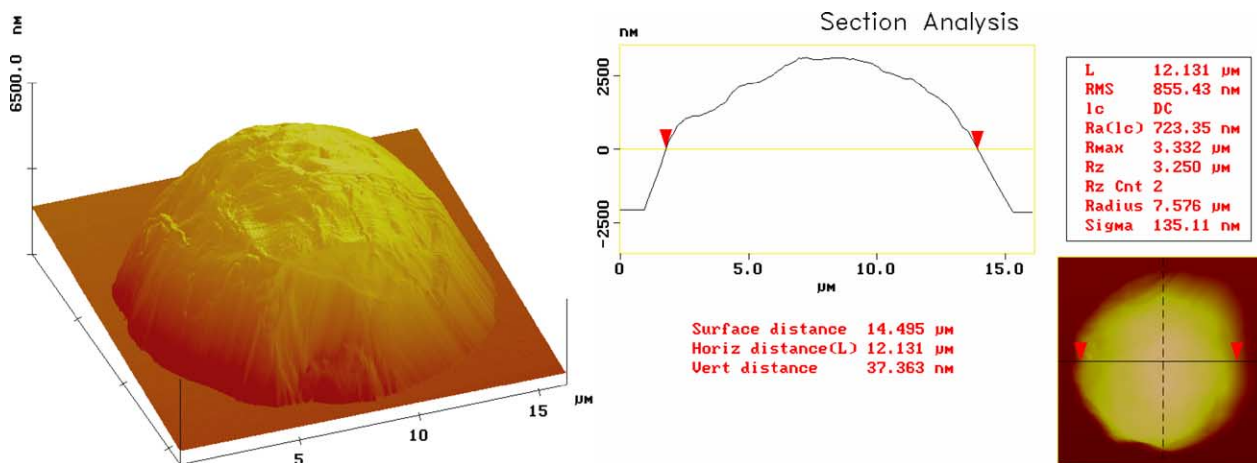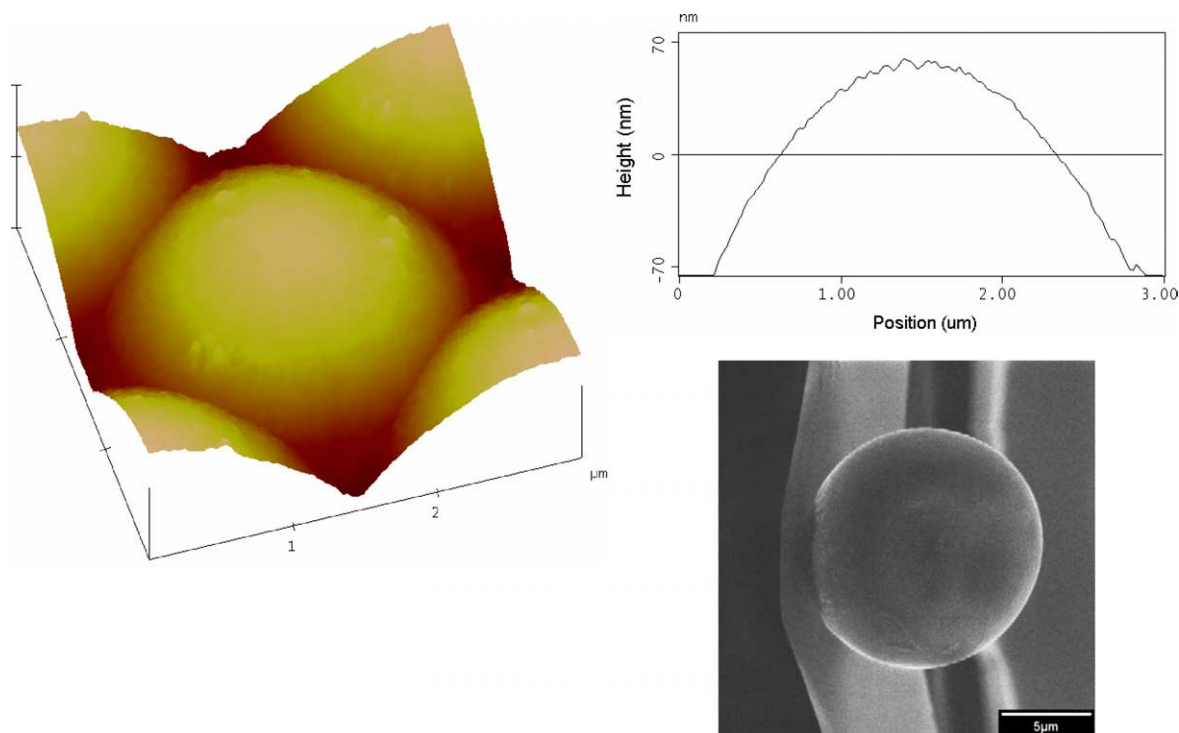

Fig. 3. Three-dimensional image of the apex of a 12-μm-diameter polyethylene microsphere attached to an AFM cantilever and a cross-sectional view of this particle. The SEM micrographs for similar particles are presented in [37].

Fig. 4. On the left: three-dimensional AFM image of the $\sim$3 $\times$ 3 µm area of the 10 µm colloidal probe (borosilicate glass) obtained by the blind tip reconstruction method (left image) during scanning over the array of spikes separated by 3 µm from each other. The graph on the right represents a cross section of this AFM image. The picture at the bottom shows the SEM micrograph of the probe (note that the nanoroughness recorded on the AFM image is indistinguishable from the SEM micrograph due to a low resolution of the picture).

An analysis performed by Maugis and Pollock [43] indicated that the applied load (P_p) for inducing full plasticity (irreversible deformation) of the particle with radius R is given by the equation

$$P_p = 10800\,\pi \frac{R^2 Y^3}{E^2}, \tag{12}$$

and the radius of the circle of contact between particle and substrate during full plasticity can be predicted from

$$a_p = 60 \frac{RY}{E}, \tag{13}$$

where E is the Young's modulus and Y is the yield strength for the material.

Knowing the probe radius of curvature (R) and mechanical properties of material (Y, E), the maximum load that can be applied in pull-off force experiments without inducing plastic deformation can be predicted from Eq. (12). For example, consider a sharp cantilever tip coated with a thick film of gold ($E = 77.5$ GPa, $Y = 0.2$ GPa, $\nu = 0.42$). For $R = 50$ nm, the full plasticity of gold will be reached at loads of $P_p = 113$ nN ($a_p = 7.7$ nm) or larger. For the commonly used V-frame cantilever with a spring constant of 0.58 N/m, the cantilever's mechanical bending of 0.2 µm in the constant compliance region of AFM force mode operation is sufficient to reach this level of loading. This clearly indicates that deformation of the sharp probes, or at least irregularities present on the probe apex [28,43,44], should be a common

phenomenon during the pull-off force measurements. The solution to this problem can be the use of larger diameter probes.

Two drawbacks must be considered however, before switching to larger probes. First, larger probes are more likely to have rough surfaces and if brittle, the nanoroughness will reduce the probe–substrate contact area, and therefore complicate interpretation of the measured pull-off forces. With soft materials, the nanoroughness of the probe may not be a problem as surface asperities can deform during pull-off force measurements, as discussed in the next part of this paper. Second, the pull-off forces increase with the size of the probe (see Eq. (4)) and larger probes need to be attached to cantilevers with larger spring constants. It is important to select new cantilevers with a spring constant that scales approximately with the value of R, or at least less than R^2. Otherwise, if k scales with R^2 (or larger), the same (or worse) problems of probe deformation will be experienced.

Adhesion forces alone can cause plastic deformation of material. Using the model presented in [43], the radius of the probe below which fully plastic deformation occurs can be calculated as

$$R \approx 1.5 \times 10^{-4} \frac{W_A E^2}{(1 - \nu^2)^2 Y^3}. \tag{14}$$

Consider a colloidal probe made of polystyrene ($\nu = 0.33$, $E = 2.55$ GPa, $Y = 10.8$ MPa) that is pressed against
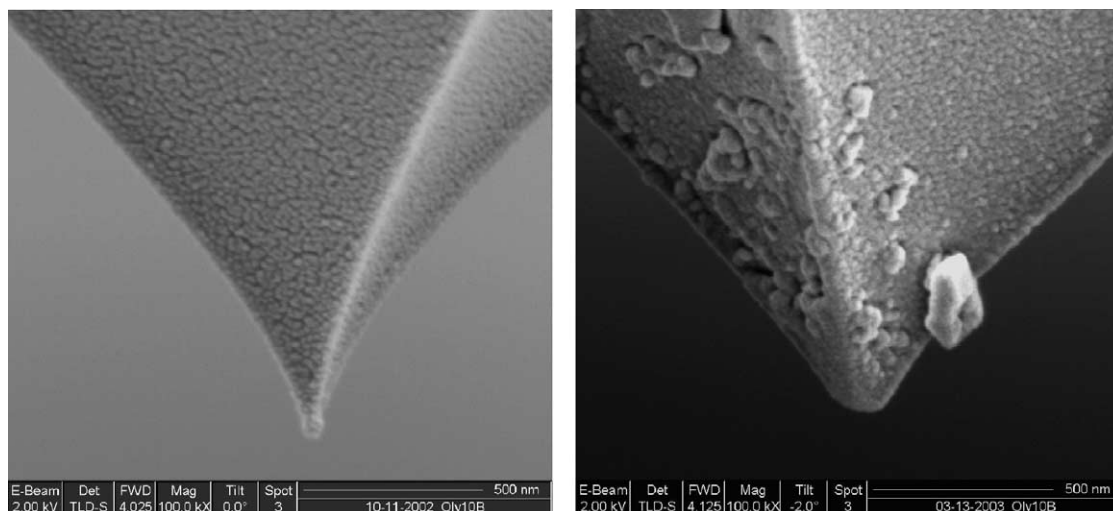
Fig. 5. Field-emission scanning electron micrograph of a tip before and after use. The right picture shows that the tip was damaged (plastically deformed) and contaminated during pull-off force measurements.

mica ($W_A = 120$ mJ/m^2) as studied in [28]. According to Eq. (14), the polystyrene probe will deform plastically if $R \leqslant 117$ nm. Colloidal probes this small made of polymer are not used in AFM pull-off force measurements. Nevertheless, these calculations indicate that any topographic irregularities on the probe surface that have a radius of curvature smaller than 117 nm can be deformed during adhesive polystyrene–mica contact. The experimental results presented in the literature support this possibility [28,44].

5.3. Substrate/probe imperfections: size limits

Contamination of a probe and a substrate by particulates and adsorbates is a common problem in the AFM laboratories. It is important to recognize that all pull-off force measurements should be done with cleaned surfaces. Cleaning the probe is usually a bigger challenge than cleaning the substrates. Fig. 6 shows two images of borosilicate glass probes; one probe had been imaged before cleaning and another one after cleaning in a surfactant solution, water, and organic solvent. Severe contamination of the glass bead shown in Fig. 6 was the result of static charge effects between dried dust particles and glass. Surface contamination by dust particles is difficult to avoid during the probe preparation/gluing, cantilever's storage and use (particles purchased from the vendor that are used for preparation of colloidal probes may already be contaminated).

Cleaning procedures should differ for each probe and substrate. Such effects as dissolution of glue by solvent, etching or dissolution of the probe/substrate surface, change in probe/substrate surface functionality, or chemical adsorption should be taken into consideration before selecting solvents and cleaning conditions.

Surface defects such as roughness and heterogeneity (inherent or introduced by adsorbed/deposited species) are serious problems in the determination of the solid surface ten-

sion by the AFM technique. Due to the small dimensions of the probes, both nanoroughness and nanoheterogeneity influence the measured pull-off forces. There was neither experimental or theoretical research done that could lead to determination of the size of surface imperfections and contamination, which affects the value of pull-off forces to such a degree that the calculated solid's surface tension (or work of adhesion) is not reliable for a particular material. In the next part of this section, we present simple models, which could be used for this purpose.

5.3.1. Roughness

It is well recognized that substrate roughness, for which asperities' dimensions are comparable or smaller to the dimensions of the probe, as well as any surface roughness at the probe apex, can affect the sphere–flat contact area to a degree that is not taken into account by simple contact mechanics models discussed thus far. If this happens, interpretation of the pull-off forces is difficult or even impossible. Both microscopic and submicroscopic roughness effects can be eliminated in many experiments by appropriate selection and preparation of the substrates. Nanoroughness of colloidal probes and/or substrates often cannot be avoided. Nevertheless, as discussed in the literature [28,29,44], nanoscale asperities can be squeezed and flattened out during the pull-off force measurements to such a degree that the probe–substrate contact area is the same as predicted by one of the contact mechanics models (usually JKR or MD model for colloidal probes). In order to reach such experimental conditions, stiff cantilevers and higher loads need to be used in the AFM pull-off force measurements [29].

We expect that the asperity may be flattened out by applying a sufficient load to initiate its plastic deformation. Therefore, if we adopt the Maugis–Pollock analysis [43], Eq. (12) predicts that at a specified load P, asperities with
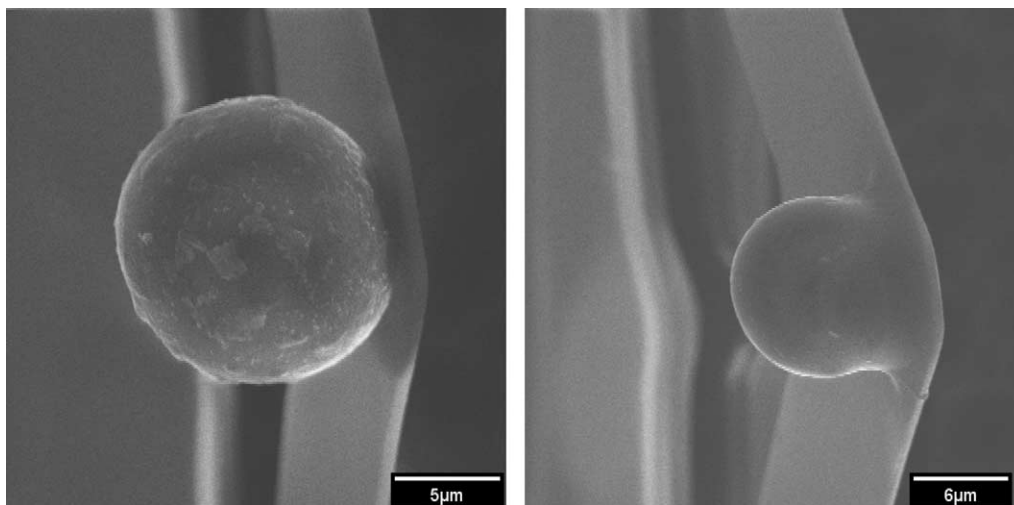
Fig. 6. Scanning electron micrographs of a colloidal probe (borosilicate glass bead) glued to a tipless cantilever before cleaning (left) and after cleaning (right).

radius of curvature of R_a and smaller will flatten out:

$$R_a \leqslant \sqrt{\frac{PE^2}{10800\,\pi\,Y^3}}. \tag{15}$$

It is also possible that asperities of a certain size and shape may deform elastically to such a degree that a probe establishes its full contact area with a substrate during loading and fully recover elastically after the probe–substrate contact is broken, if sufficient time for this recovery is allowed. This will happen if elastic deformation (δ) is comparable to the height of asperity (h); $\delta \geqslant h$. This means that only asperities with a radius of curvature much larger than the height of the asperity can experience such deformation. If this possibility is analyzed in view of the JKR model [10], we conclude that

$$h \leqslant \frac{a^2}{R_a} - \frac{2}{3}\sqrt{\frac{6\pi a W_A}{K}}, \tag{16}$$

where

$$a = \sqrt[3]{\frac{R_a}{K}\Big[P + 3\pi R_a W_A + \sqrt{6\pi R_a W_A P + (3\pi R_a W_A)^2}\,\Big]}. \tag{17}$$

Consider, for example, a polymeric probe interacting with a rigid material. Assuming that asperities on the probe surface have radii of $R_a = 100$ nm, and the system is characterized by the following parameters: $K = 65$ GPa, $W_A = 120$ mJ/m^2, and $P = 10$ μN, we calculate that asperities with the height of $h \leqslant 6.2$ nm can be completely deformed elastically to allow for the probe–substrate contact area that is predicted by the JKR model. Alternatively, the load needed to produce a desired deformation of the surface topographic irregularities could be estimated by Eq. (16) if the dimensions of irregularities (R_a and h) are determined with the AFM or another technique.

5.3.2. Heterogeneity

Using contact mechanics models we can also estimate a maximum size of an impurity/surface heterogeneity that has a negligible effect on the measured pull-off force. In most of the systems this will occur if the impurity and/or heterogeneity has a dimension (d) smaller than 10% of the probe–substrate contact area at zero load conditions, $(\pi d^2)/4 < (0.1\pi a_0^2)$, and therefore $d < 0.63 a_0$, where a_0 is the probe–substrate contact radius at zero load. Assuming also that the system meets the terms of the DMT model, the size (diameter) of the heterogeneity/impurity that can be accepted in the pull-off force measurements can be estimated from the following equation:

$$d < 0.63 \sqrt[3]{\frac{2\pi R^2 W_A}{K}}. \tag{18}$$

For example, for $R = 50$ nm, $W_A = 100$ mJ/m^2, $K = 63$ GPa (which are characteristic values determined for sharp tips coated with a gold film and modified with SAMs of thiols [45]), the heterogeneity with a diameter as small as 1.8 nm will influence the measured pull-off force. This means that a few molecular defects in the structure of SAMs, which are common for thiol monolayers aligned into domains on gold surfaces [46], most likely affect the magnitude and variation of measured pull-off forces, and one (reproducible) pull-off force value is almost impossible to obtain experimentally for such systems. Replacement of the sharp probe with a 10-μm-diameter colloidal probe, which more likely will operate in the regime described by the JKR model (therefore, factor 2 must be replaced with 6 under the square root in Eq. (18)), will increase this limit to about 90 nm. The heterogeneity size of less than 90 nm is more realistically avoidable in routine pull-off force measurements and the use of larger probes seems to be more appropriate in γ determination, from the prospective of surface heterogeneity. Problem is that colloidal probes of perfect sphericity with smooth surfaces are difficult to manufacture. Nevertheless, as discussed in the previous section, nanoroughness of soft probes (and substrates) can be flattened out during pull-off force measurements reducing or eliminating the ef-

fect of roughness on probe–substrate contact area. The same "trick," however, cannot be imposed on hard materials.

6. Can solid surface tension be determined for rough surfaces?

The factor that complicates interpretation of the measured AFM pull-off forces the most is surface roughness. Quantitative calculations of the adhesion force between a particle and rough surface are difficult for many reasons. The size, shape, homogeneity, mechanical properties and distribution of the asperities (deviations from an ideal planar surface) influence the actual area of contact, and therefore directly affect the pull-off force [39,45,47]. The particle can also have an irregular geometry leading to more difficulties in quantitative analysis of pull-off force data [39] but this case is not discussed here.

Surface roughness causes the actual area of contact to vary significantly from the ideal spherical particle on flat surface contact. Roughness can increase the adhesion of particles to a surface or decrease it depending on the scale of the roughness, location on the surface where contact is made, and the size and geometry of the particle.

The actual area of contact between a particle and rough surface depends on the size and distribution of the asperities on the surface [39,45]. The probe–substrate contact area often increases for probes whose size is smaller than the distance between asperities of a microscopically rough surface. However, the increased area of adhesion between the probe and rough surface can also result from multiple probe–substrate contacts, if the probe only partially penetrates the space between asperities and interacts with the walls of two or more asperities [45]. Multi-modal distribution of pull-off forces can be recorded for such systems. It should be recognized however, that the appearance of multi-modal distribution of pull-off forces does not necessarily indicate that the multiple contact points are experienced during the pull-off force measurements. Surface heterogeneity is another cause for generation of similar graphs and therefore results similar to those presented in [45] should be interpreted with caution.

When the size of the probe is larger than the distance between asperities, the probe cannot penetrate the interasperity space and the contact area between probe and substrate is reduced. As a result, the pull-off forces are weaker than expected for the sphere–flat geometry. Two different scenarios are possible in such a sphere–rough surface system. First, as discussed earlier, if the loads applied during probe–substrate contact are increased to high values, elastic and/or plastic deformation of asperities can be induced. For applied loads that are properly managed, the probe–substrate contact area corresponds to that predicted by contact mechanics of sphere–flat geometry system.

In many systems, however, sufficient deformation of asperities cannot be initiated due to the low stiffness of available/used cantilevers and high hardness of materials used in experiments. For these systems, the work of adhesion between the probe and a submicroscopically rough substrate can still be estimated from the measured pull-off forces. This is possible with the theoretical model recently introduced by Rabinovich et al. [48]. Assumptions and details of the mathematics of the Rabinovich model will not be repeated here and only final equation is presented:

$$W_A = \left(\frac{F}{R} - B \right) \frac{58 R \, \mathrm{rms}_2}{c \pi \lambda_2^2}, \tag{19}$$

where

$$B = \frac{A}{6 z_0^2} \frac{1}{(1 + 58 R \, \mathrm{rms}_1 / \lambda_1^2)(1 + 1.82 \, \mathrm{rms}_2 / z_0)^2}, \tag{20}$$

$$\mathrm{rms} = \sqrt{\frac{32 \int_0^r y^2 r_1 \, dr_1}{\lambda^2} k_p}; \tag{21}$$

c is constant equal to $c = 1.5$ if JKR contact mechanics apply and $c = 2$ if DMT contact mechanics apply (note that in original paper by Rabinovich et al. [48] $c = 1.5$); λ is the peak-to-peak distance between asperities ($\lambda = 4r$); k_p is the surface packing density for close-packed spheres ($k_p = 0.907$); A is the Hamaker constant; z_0 is the distance of closest approach between the two surfaces; r and R are the radius of the asperity and particle, respectively; k_1 is a coefficient relating the rms roughness and the maximum peak height, which is equal to 1.817 for the assumed geometry. The model geometry is shown in Fig. 7.

In this model, surfaces which exhibit two scales of roughness, both smaller than the size of spherical probe, are considered (Fig. 7). The first type of roughness, called rms_1, is associated with a longer peak-to-peak distance, λ_1. A second smaller roughness, called rms_2, is associated with a smaller peak-to-peak distance, λ_2.

Because for many systems $F/R \gg B$, Eq. (19) can be reduced to

$$W_A = \frac{58 F \, \mathrm{rms}_2}{c \pi \lambda_2^2}. \tag{22}$$

Again, if both probe and substrate are made of the same material,

$$\gamma_S = \frac{29 F \, \mathrm{rms}_2}{c \pi \lambda_2^2}. \tag{23}$$

To test the Rabinovich model we analyze the results of pull-off forces measured for silanized glass probes in contact with rough polypropylene substrates and reported in [39]. Table 4 lists substrate characteristics, measured (average) pull-off forces, and calculated values of the work of adhesion. The work of adhesion was calculated using Eq. (4) assuming $c = 1.6$. Three polypropylene substrates of very random roughness, regarding the size of asperities and their distribution, which as reported earlier [39] did not fit to the Rabinovich model, are not included in the presented analysis.
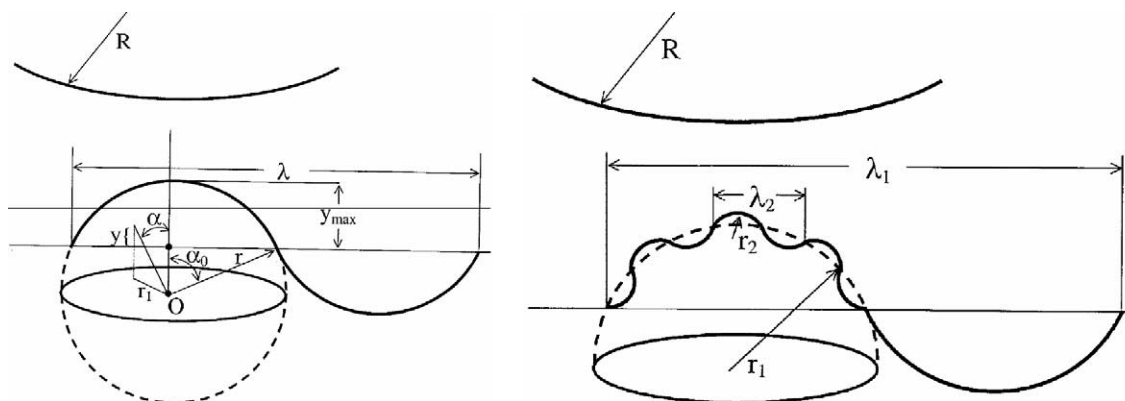
Fig. 7. Rabinovich's model geometry for surfaces having two different scales of roughness.

Table 4
Surface roughness of polypropylene samples, average pull-off forces between polypropylene and silanized glass probe [39], and calculated polypropylene-silanized glass work of adhesion

Sample	Surface roughness characteristics				Pull-off force [nN]	Work of adhesion [mJ/m^2]	
	rms$_1$ [nm]	λ_1 [μm]	rms$_2$[nm]	λ_2 [nm]		Exp.	Theor.
1	25	3.7	6.5	366	76	42	
2	42	4.5	15.6	598	136	68	
3	386	5.8	39.6	964	100	49	48–54[a]
4	194	7.5	32.6	685	41	33	
5	31	3.1	13.6	548	74	38	
6	37	3.9	16.0	345	63	98	
					Average:	55 (49)[b]	~50

[a] Estimated using $W_A \approx 2(\gamma_1\gamma_2)^{1/2}$, where $\gamma_1 = 25.7$ mJ/m^2 is the surface tension of polypropylene [3], and $\gamma_2 = 22–28$ mJ/m^2 is the surface tension of silanized glass (own data).

[b] In parentheses: average value calculated for four samples, without result for samples 4 and 6.

As shown in Table 4, an average value of the work of adhesion between polypropylene and silanized glass, calculated from the Rabinovich model, relates well to the theoretical value estimated from the surface tensions of interacting surfaces.

7. Concluding remarks

The atomic force microscopy is commonly used in measurements of particle–substrate adhesion through pull-off force measurements, and the measured pull-off force values are used to determine the work of adhesion (W_A) and/or solid's surface tension/surface energy (γ). However, the experimental results presented in the literature over the last several years indicate inconsistency and poor reproducibility of pull-off forces measured with the AFM technique. The scatter and irreproducibility of the experimental results is mainly caused by variation in solid surface roughness and heterogeneity characteristics (that of probe and substrate) and these characteristics should be analyzed and reported. As demonstrated in this paper, imperfections and defects of the interacting surfaces as small as a few angstroms can substantially influence the measured pull-off force, particularly for small probes made of rigid material. The use of

larger probes reduces the detrimental effects of molecular heterogeneity on the measured pull-off force, but conversely, increases the danger that surface roughness will reduce the probe–substrate contact area.

Varying loading conditions imposed on a probe by the deflected cantilever during the pull-off force measurements can be another source of pull-off force variation. Loads should be managed properly to avoid plastic deformation or damages to rigid probes. On the other hand, deformations of the nanoscaled surface irregularities of compliant materials, managed by increased loads, can reduce or even eliminate the effects of nanoroughness on the probe–substrate contact area, promoting conditions described by the contact mechanics models for the sphere–flat system.

Determination of W_A and γ from pull-off force measurements has been practiced over the last several years using contact mechanics theoretical models derived for sphere–flat systems. Unfortunately, the theoretical models were often selected without careful analysis of both the experimental system and theoretical model. A majority of the literature solid's surface tension results was obtained using either JKR or DMT models, although our re-analysis of the published experimental data indicates that these models were misused and very often should be replaced with the Maugis–Dugdale (MD) model. As a result, many published W_A and γ data

should be regarded with caution. It is also important that further research on pull-off force measurements be continued but under more restricted experimental conditions.

The analysis of pull-off forces measured for rigid substrates and probes having nanoroughness characteristics in terms of W_A and γ still seems possible if probes selected are much larger than the size of roughness features of interacting surfaces. In order to succeed with interpretation of such complex systems, a detailed surface analysis in term of roughness parameters, asperity size and shape, and spacing between asperities is required. Then, analysis of the experimental data should be done with one of the theoretical models, which is suitable for rough surfaces; the model proposed by Rabinovich et al. [48] is the most promising one at this time.

Acknowledgment

References

[1] A.I. Rusanov, V.A. Prokhorov, Interfacial Tensiometry, Elsevier, Amsterdam, 1996.

[2] H.-J. Butt, R. Raiteri, in: A.J. Milling (Ed.), Surface Characterization Methods: Principles, Techniques, and Applications, Dekker, New York, 1999, pp. 1–36.

[3] C.J. Van Oss, Interfacial Forces in Aqueous Media, Dekker, New York, 1994.

[4] B. Cappella, G. Dietler, Surf. Sci. Rep. 34 (1999) 1–104.

[5] D. Sarid, Scanning Force Microscopy, Oxford Univ. Press, New York, 1991.

[6] R. Wiesendanger, Scanning Probe Microscopy and Spectroscopy: Methods and Applications, Cambridge Univ. Press, Cambridge, 1994.

[7] J.E. Sader, in: Encyclopedia of Surface and Colloid Science, Dekker, 2002, pp. 846–856.

[8] J.P. Cleveland, S. Manne, D. Bocek, P.K. Hansma, Rev. Sci. Instrum. 64 (1993) 403–405.

[9] J.L. Hutler, J. Bechhoefer, Rev. Sci. Instrum. 64 (1993) 1868–1873.

[10] K.L. Johnson, K. Kendall, A.D. Roberts, Proc. R. Soc. London A 324 (1971) 301–313.

[11] B.V. Derjaguin, V.M. Muller, Y.P. Toporov, J. Colloid Interface Sci. 53 (1975) 314–326.

[12] D. Maugis, Contact, Adhesion and Rupture of Elastic Solids, Springer, Berlin, 2000.

[13] N.A. Burnham, A.J. Kulik, in: B. Bhushan (Ed.), Handbook of Micro/Nano Tribology, second ed., CRC Press, Boca Raton, 1999, pp. 247–271.

[14] O. Marti, in: B. Bhushan (Ed.), Modern Tribology Handbook, vol. I, CRC Press, Boca Raton, 2001, pp. 617–639.

[15] U.D. Schwarz, J. Colloid Interface Sci. 261 (2003) 99–106.

[16] D. Maugis, J. Colloid Interface Sci. 150 (1992) 243–269.

[17] H. Hertz, Miscellaneous Papers, Macmillan, London, 1896.

[18] R.W. Carpick, D.F. Ogletree, M. Salmeron, J. Colloid Interface Sci. 211 (1999) 395–400.

[19] A. Noy, C.D. Friesbie, L.F. Rozsnyai, M.S. Wrighton, C.M. Lieber, J. Am. Chem. Soc. 117 (1995) 7943–7951.

[20] E.W. Van der Vegte, G. Hadziioannou, Langmuir 13 (1997) 4357–4366.

[21] V.V. Tsukruk, V.N. Bliznyuk, Langmuir 14 (1998) 446–455.

[22] S.C. Clear, P.F. Nealy, J. Colloid Interface Sci. 213 (1999) 238–250.

[23] A. El Ghzaoui, J. Appl. Phys. 85 (1999) 1231–1233.

[24] H. Skulason, C.D. Friesbie, Langmuir 16 (2000) 6294–6297.

[25] C. Jacquot, J. Takadoum, J. Adhes. Sci. Technol. 14 (2001) 681–687.

[26] F.L. Leite, A. Riul Jr., P.S.P. Herrmann, J. Adhes. Sci. Technol. 17 (2003) 2141–2156.

[27] N.A. Burnham, D.D. Dominguez, R.L. Mowery, R.J. Colton, Phys. Rev. Lett. 64 (1990) 1931–1934.

[28] S. Biggs, G. Spinks, J. Adhes. Sci. Technol. 12 (1998) 461–478.

[29] J. Nalaskowski, J. Drelich, J. Hupka, J.D. Miller, Langmuir 19 (2003) 5311–5317.

[30] Web site: http://www.webelements.com.

[31] J.R. Fried, Polymer Science and Technology, Prentice–Hall PTR, New Jersey, 1995.

[32] H. Matsuoka, T. Kato, Adhesion forces between mica surfaces in air and liquids, in: International Tribology Conference, Yokohama, 1995.

[33] M. Barsoum, Fundamentals of Ceramics, McGraw–Hill, New York, 1997.

[34] W.D. Callister Jr., Materials Science and Engineering. An Introduction, fourth ed., Wiley, New York, 1997.

[35] A. Noy, D.V. Vezenov, C.M. Lieber, Ann. Rev. Mater. Sci. 27 (1997) 381–421.

[36] E. Beach, G. Tormoen, J. Drelich, J. Adhes. Sci. Technol. 16 (2002) 845–868.

[37] J. Nalaskowski, J. Drelich, J. Hupka, J.D. Miller, J. Adhes. Sci. Technol. 13 (1999) 1–17.

[38] J. Drelich, J. Nalaskowski, J.D. Miller, J. Colloid Interface Sci. 201 (1998) 253–256.

[39] E.R. Beach, G.W. Tormoen, J. Drelich, R. Han, J. Colloid Interface Sci. 247 (2002) 84–99.

[40] L.H.G.J. Segeren, B. Siebum, F.G. Karssenberg, J.W.A. van den Berg, G.J. Vancso, J. Adhes. Sci. Technol. 16 (2002) 793–828.

[41] R. Chi, Z. Xu, T. DiFeo, J.A. Finch, J.L. Yordan, J. Pulp Paper 27 (2001) 152–159.

[42] J.S. Villarubia, J. Res. Natl. Inst. Stand. Technol. 102 (1997) 425–454.

[43] D. Maugis, H.M. Pollock, Acta Metall. 9 (1984) 1323–1334.

[44] E.R. Beach, J. Drelich, in: J.J. Kellar, M.A. Herpfer, B.M. Moudgil (Eds.), Functional Fillers and Nanoscale Minerals, Society for Mining, Metallurgy, and Exploration, Littleton, CO, 2003, pp. 177–193.

[45] G.W. Tormoen, J. Drelich, E.R. Beach, J. Adhes. Sci. Technol. 8 (2004) 1–18.

[46] C. Schonenberger, J. Jorritsma, J.A.M. Sondag-Huethorst, L.G.J. Fokkink, J. Phys. Chem. 99 (1995) 3259–3271.

[47] L. Sirghi, N. Hakagiri, K. Sugisaki, H. Sugimura, O. Takai, Langmuir 16 (2000) 7796–7800.

[48] Y.I. Rabinovich, J.J. Adler, A. Ata, R.K. Singh, B.M. Moudgil, J. Colloid Interface Sci. 232 (2000) 17–24.